Electrochemistry
The Electrochemical Society of Japan
Received: November 5, 2021
Accepted: November 30, 2021
Published online: December 3, 2021
Issued: January 15, 2022
https://doi.org/10.5796/electrochemistry.21-00115
https://doi.org/10.50892/data.electrochemistry.17109038
Article
Electrochemistry, 90(1), 017008 (2022)

Electrochemical Performance of Nanorod-like (La, Zr) Co-Doped Li-rich $Li_{1.2}Ni_{0.2}Mn_{0.6}O_2$ Cathodes for Use in Lithium-Ion Batteries

Wencong WANG,[a,b] Hiromasa HANZAWA,[a] Ken-ichi MACHIDA,[a] Kohei MIYAZAKI,[b,*,§] and Takeshi ABE[b,§]

[a] Graduate School of Engineering, Osaka University, 2-1 Yamadaoka, Suita, Osaka 565-0871, Japan
[b] Graduate School of Engineering, Kyoto University, Katsura, Nishikyo-ku, Kyoto 615-8510, Japan

* Corresponding author: myzkohei@elech.kuic.kyoto-u.ac.jp

ABSTRACT

A lithium-rich layered structure in lithium-ion batteries (LIBs) has attracted much attention due to its high capacity of over 250 mAh g^{-1} after activation. This could satisfy the requirements of next-generation energy-storage devices. However, a spinel-like impurity phase that forms from the pristine layered structure during cycling is considered to be harmful to the structure stability and Li^+ mobility, resulting in undesired electrochemical performance. In this study, nanorod-like $Li_{1.2}Ni_{0.2}Mn_{0.6}O_2$ with a three-dimensional architecture was synthesized by evaporative-crystallization with as-prepared nano-MnO_2 as a hard template. The structure stability and Li^+ mobility of the nanorod-like $Li_{1.2}Ni_{0.2}Mn_{0.6}O_2$ was improved by the addition of an appropriate molar ratios of (La, Zr) co-dopants. This combination exhibited outstanding capacity retention of 80.9 % with a stable discharge capacity of 102 mAh g^{-1} after 300 cycles under a high current density of 1000 mA g^{-1} (corresponding to 5 C). This study suggests that the use of a multi-prong strategy that combines morphology control and co-doping should be an effective method for improving the high-rate performance of Li-rich materials.

Keywords : Li-rich Layered Cathodes, Doping, Nanorod, High-rate Performance

1. Introduction

Recently, as a result of pressure to achieve carbon-neutrality and the global energy crisis, renewable clean energy from natural sources without the emission of greenhouse gases, such as solar energy, wind energy and geothermal energy, has attracted much attention. As our energy infrastructure changes to include more renewable energy, energy-storage devices with stable storage capability and high conversion efficiency are urgently needed. Rechargeable lithium-ion batteries (LIBs) are a prevalent energy-storage device that have been applied in numerous smart portable devices because of their high energy-conversion efficiency based on an electrochemical reaction, low self-discharge, high energy density and long-life performance. However, to meet the ballooning need for energy storage next-generation LIBs with an even higher energy density will be needed.[1] To increase the energy density of LIBs, Li-rich cathode material with a formula of $Li_{1+x}M_{1-x}O_2$ ($0 < x < 1/3$), which can be denoted as $xLi_2MnO_3 \cdot (1-x)LiMO_2$ (M = Mn, Ni, etc.), exhibits prominent specific capacity over 250 mAh g^{-1} after activation by charging to a high potential (≥4.5 V).[2,3] $xLi_2MnO_3 \cdot (1-x)LiMO_2$ contains two kinds of similar layered structures corresponding to the monoclinic phase ($C2/m$ space group) and rhombohedral phase ($R\bar{3}m$ space group). $Li_{1.2}Ni_{0.2}Mn_{0.6}O_2$, as a typical Li-rich material derived from Li_2MnO_3, can be described by a composite structure of $0.5Li_2MnO_3 \cdot 0.5LiMn_{0.5}Ni_{0.5}O_2$, in which some of the Mn^{4+} and Li^+ in the transition metal layer are replaced by Ni^{2+} while the residual Mn atoms remain in a stable oxidation state of 4+.[4–6] The structure of Li_2MnO_3 can also be presented in a layered formation, denoted as $Li[Li_{1/3}Mn_{2/3}]O_2$, in which one third of the transition metal layer is occupied by lithium atoms and thus the transition metal atoms in octahedral sites are transferred into a distorted structure with close-packed oxygen arrays, which makes it difficult to analyze the structure.[7] Thackeray and co-workers first reported lithium manganese oxide with a chemical formula of $Li_{0.36}Mn_{0.91}O_2$ by acid-leaching of Li_2O from Li_2MnO_3; its lithiated structure of $Li_{1.09}Mn_{0.91}O_2$ is relatively stable.[8,9] Subsequently, Kalyani and co-worker also suggested that Li_2MnO_3 could be used as a 3 V-positive material.[10] To date, Li-rich material has been the focus of considerable effort in many studies to achieve better electrochemical stability, due to the inferior kinetics of Li-ion diffusion and the gradual increase in a spinel-like phase transformed from the pristine layer structure by a loss of oxygen during cycling.[11–13] Doping with heteroatoms could be an effective strategy, and has frequently been reported in the literature.[14–19] Na^+, K^+, Cr^{3+}, Nb^{5+}, and Mo^{6+} with different chemical valence to substitute for some Li^+ or Mn^{4+} atoms have been shown to stabilize the host layered structure and suppress the phase transformation to form spinel-like phases and thus improve the cycling stability and rate performance. In addition, modification of the morphology of the three-dimensional architecture of Li-rich material could be an effective method for enhancing the electrochemical performance. Chen and co-workers designed a 3D reticular structure of $Li_{1.2}Ni_{0.2}Mn_{0.6}O_2$ with mesoporous silica as a hard template that showed stable cycling at 1 C with remarkable capacity retention.[20] Wu and co-workers synthesized $Li_{1.2}Ni_{0.2}Mn_{0.6}O_2$ nanoplates and modulated the structure to expose the electrochemically active 010 planes and achieve excellent cycling stability.[21]

In this study, nanorod-like Li-rich $Li_{1.2}Ni_{0.2}Mn_{0.6}O_2$ with a three-dimensional architecture was prepared by using nano-MnO_2 precursor as a hard template. To further improve the Li ion conductivity of the Li-rich structure, heteroatoms with different molar ratios of (La, Zr) as co-dopants were adopted. After doping with appropriate amounts of the (La, Zr) co-dopants, the electrode with a nanorod-like Li-rich structure showed much higher capacity retention and rate performance compared to a pristine electrode.

§ECSJ Active Member
K. Miyazaki orcid.org/0000-0001-5177-3570
T. Abe orcid.org/0000-0002-1515-8340

2. Experimental

2.1 Material preparation

2.1.1 Synthesis of a nanorod-like MnO_2 precursor

Nanorod-like MnO_2 was fabricated by a typical hydrothermal method, using 0.826 mL HCl (Wako) and 45 mL distilled water as a reaction solution; 2.5 mmol $KMnO_4$ was added to the pre-mixed solution with vigorous stirring at room temperature for over 1 h before it was transferred to a Teflon-lined stainless autoclave followed by heat treatment at 140 °C for 12 h. The black precipitate was collected and washed several times with ethanol and distilled water to remove the residue products until it reached neutral pH, followed by drying under vacuum at 100 °C for 12 h.

2.1.2 Synthesis of a nanorod-like Li-rich $Li_{1.2}Ni_{0.2}Mn_{0.6-x}(La, Zr)_xO_2$ co-doped structure

The as-prepared MnO_2 precursor was first dispersed in 5 mL ethanol with $Ni(NO_3)_2{\cdot}6H_2O$ (99.9 %, Wako) in a stoichiometric proportion. The solution was then heated at 40 °C to evaporate the solvent. After evaporation, the mixture was heated at 300 °C for 2 h and at 500 °C for 3 h in a muffle furnace under air atmosphere to form pre-oxide powder. This powder was re-dispersed in ethanol and mixed with $LiNO_3$ (Wako) in a molar ratio of 1 : 1.05, and pressed into pellet, in which an excess of lithium was used to compensate for the lithium lost during annealing at high temperature. The pellet was annealed at 500 °C for 3 h and finally crystallized at 850 °C for 10 h with a heating rate of 2 °C/min. The annealing procedure for preparing the (La, Zr) co-doped Li-rich materials was similar. Different concentrations of $La(NO_3)_2{\cdot}6H_2O$ (Wako) and $ZrO(NO_3)_2{\cdot}2H_2O$ (Wako) in ethanol were used as dopants to mix with the nickel source before being pressed into pellets. The molar ratios of dopants (La and Zr) were fixed at 3 : 2 in the following discussion. The Li-rich structures doped with La and Zr are denoted as $Li_{1.2}Ni_{0.2}Mn_{0.6-x}(La, Zr)_xO_2$, where x (0.005, 0.01, and 0.02) refers to the molar ratios of co-dopants.

2.2 Material characterization

Powder X-ray diffraction (XRD, Rigaku RINT2200, Japan) equipped with monochromatic CuKα radiation ($\lambda = 1.54$ Å) under conditions of 40 kV, 30 mA was carried out to identify the phase transition in the Li-rich structure affected by doping with various amounts of dopants. A detailed structure analysis was performed over a range of 10° to 80° with a scan rate of 2° per min. Scanning electron microscopy (SEM, Hitachi S-3000) was used to investigate the change in morphology during the annealing process.

2.3 Electrochemical measurements of the electrodes

To evaluate the electrochemical performance of the synthesized Li-rich materials, a half-cell (Hohsen, Japan) with lithium metal foil as a counter electrode and Celgard 2500 as a separator was assembled and sealed in an argon glove-box ($O_2 \leq 1$ ppm; $H_2O \leq 1$ ppm). The working electrode with aluminum as a current collector was fabricated from a slurry that contained 80 wt% of the Li-rich powder as the active material, 10 wt% conductive acetylene black, and 10 wt% polyvinylidene difluoride (PVdF) as a binder. The slurry was stirred with a suitable amount of *N*-methyl-2-pyrrolidone (NMP) as a solvent and pasted on the aluminum foil with a controlled thickness of 120 µm to prepare the electrode. All of the as-prepared electrodes were dried under 120 °C for 12 h to remove the residue solvent. The electrolyte used in this experiment was 1 mol dm^{-3} $LiPF_6$ solution in ethylene carbonate (EC) and diethyl carbonate (DEC) (1 : 1 by vol., Kishida Chemical Co.). The galvanostatic charge-discharge performance was evaluated on a battery test system (CT2100A, Wuhan LAND Electronics Co., Ltd., China) in the potential range from 2.0 to 4.8 V at room temperature (25 °C), with a current density of 0.1–0.5 C (1 C = 200 mA g^{-1}). Cyclic voltammetry (CV) was conducted using an automatic polarization system (HZ5000, HOKUTO DENKO, Japan) with a scan rate of 0.1–1 mV s^{-1} between 2.0 and 5.0 V. Unless otherwise mentioned, all potentials used in this study refer to lithium metal.

3. Results and Discussion

3.1 Structure and morphology

The structural characteristics of the MnO_2 powder prepared by this hydrothermal method were determined from the XRD pattern as shown in Fig. 1a. The main reflections were well indexed to the tetragonal α-MnO_2 structure that belongs to the $I4/m$ space group (ICSD #72-1982) without any impurity phase. The SEM image in Fig. 1b shows that the MnO_2 precursor showed a sphere morphology with a diameter of around 5 µm. In addition, enlarged images in Figs. S1a and S1b clearly revealed that the sphere structure was composed of many uniform primary nanorod-like particles with a diameter of 100 nm and a length of 2–3 µm. The as-prepared MnO_2 powder with a nanorod-like structure was used to conduct the following experiments.

The as-prepared MnO_2 powder combined with $Ni(NO_3)_2$ and different molar ratios of (La, Zr) dopants of x without a lithium source was first pressed into a pellet. To clarify the growth mode of the Li-rich structure during the annealing process, SEM images of a pristine sample and samples with different molar ratios of co-dopants after pre-annealing at 500 °C are shown in Fig. 2. According to Figs. 2b–2d ($x = 0.005$, 0.01, and 0.02), even when combined with a certain amount of dopants, the primary nanorod-like particles retained their structure during pre-annealing with only an increase in diameter of around 200 nm. Notably, when the molar ratio of co-dopants was 0.02, a coarse surface of nanoparticles with a diameter of less than 50 nm growing on the nanorod-like structure was confirmed as shown in Fig. 2d. This is principally due to the

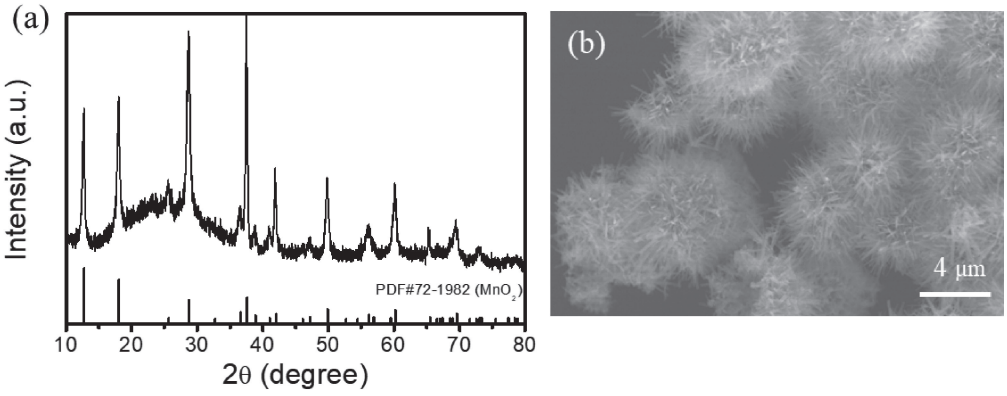

Figure 1. (a) XRD pattern and (b) SEM image of the as-prepared MnO_2 powder by hydrothermal method.

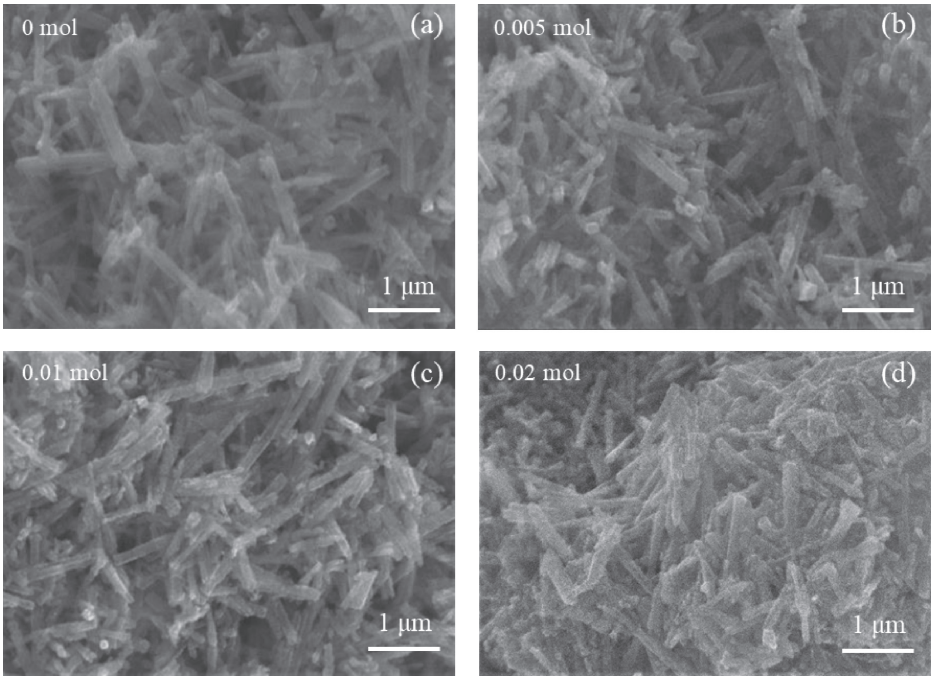

Figure 2. SEM images of the intermediate oxide with different molar ratios of (La, Zr) co-dopants, $x =$ (a) 0, (b) 0.005, (c) 0.01, and (d) 0.02, respectively, after the 500 °C pre-annealing process without lithium source.

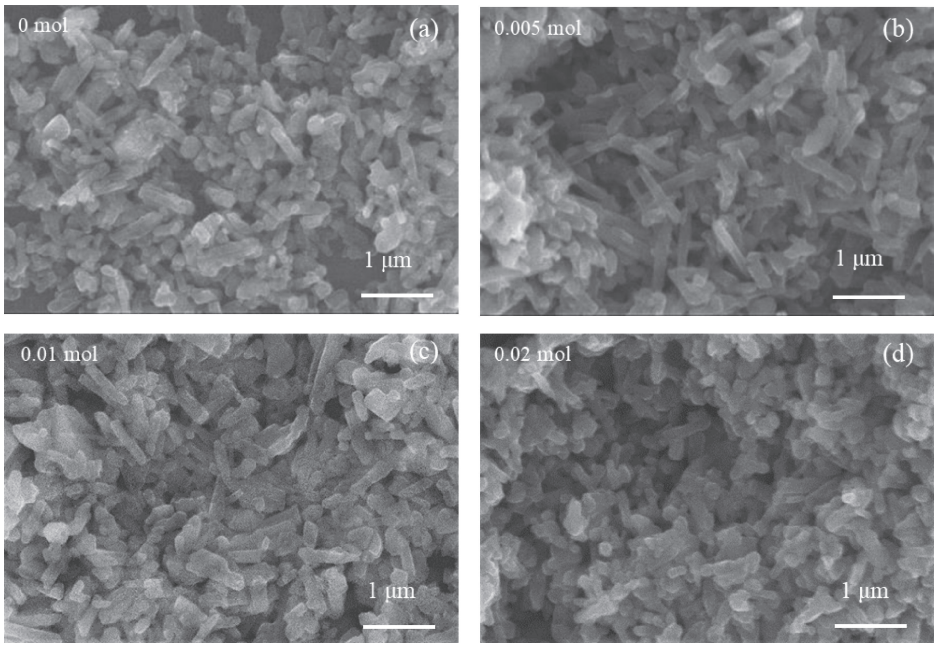

Figure 3. SEM images of nanorod-like Li-rich $Li_{1.2}Ni_{0.2}Mn_{0.6-x}O_2$ materials with different molar ratios of (La, Zr) co-dopants $x =$ (a) 0, (b) 0.005, (c) 0.01, and (d) 0.02, respectively, after the final crystallization process at 850 °C.

presence of many heteroatoms that could lead to the formation of an impurity phase. Images of Li-rich $Li_{1.2}Ni_{0.2}Mn_{0.6-x}O_2$ with different molar ratios of co-dopants after the final crystallization process are shown in Fig. 3. The Li-rich material without dopants as shown in Fig. 3a maintained a nanorod-like structure. However, some regions of collapse were also observed. For materials doped with (La, Zr) co-dopants at a low molar ratio ($x = 0.005$ and 0.01), as shown in Figs. 3b and 3c, respectively, a uniform arranged nanorod-like structure with a diameter of 200 nm and a length of 1 µm was confirmed. These nanorods contributed to a porous-like space and thus formed a three-dimensional architecture, which is beneficial to increase the contact area between active materials and electrolytes. For material doped with a high molar ratio of 0.02 (Fig. 3d), the nanorod-like structure tended to form an irregular shape compared to those with lower doping molar ratios of 0.005 and 0.01. This difference might be explained by the formation of an impurity phase with a different lattice structure. Thus, the as-prepared MnO_2 nanorod-like structure may have acted as a template that could further guide the growth of the Li-rich structure along the nanorods. However, this structure was not robust enough to absorb the stress

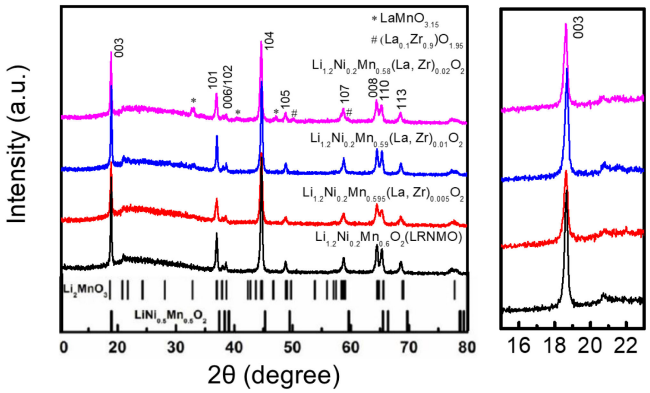

Figure 4. XRD patterns of nanorod-like $Li_{1.2}Ni_{0.2}Mn_{0.6-x}O_2$ materials with various ratios of (La, Zr) co-dopants $x = 0$, 0.005, 0.01, and 0.02, respectively, after the final crystallization process at 850 °C and the enlarged figure of the 003 plane in the right side. (*) refers to the $LaMnO_{3.15}$, (#) refers to the $(La_{0.9}Zr_{0.1})O_{1.95}$.

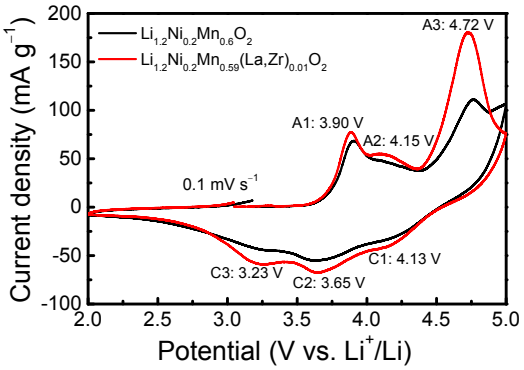

Figure 5. Cyclic voltammograms of the pristine nanorod-like $Li_{1.2}Ni_{0.2}Mn_{0.6-x}O_2$ electrode and the electrode with (La, Zr) dopants at $x = 0.01$ during the first cycle at the scan rate of 0.1 mV s^{-1}, from 2.0 to 5.0 V.

during crystallization. By doping with an appropriate molar ratio of (La, Zr) co-dopants, the Li-rich $Li_{1.2}Ni_{0.2}Mn_{0.6-x}O_2$ showed reinforced structural stability and formed a nanorod-induced three-dimensional architecture.

The XRD patterns of Li-rich $Li_{1.2}Ni_{0.2}Mn_{0.6}O_2$ materials with various molar ratios of (La, Zr) dopants are presented in Fig. 4. The main peak of the XRD pattern in the pristine sample (black line) could be well indexed to a hexagonal α-$NaFeO_2$ structure with good crystallinity. This pattern was similar to the standard pattern of $LiNi_{0.5}Mn_{0.5}O_2$ and was assigned to the space group $R\bar{3}m$ with a layered symmetry.[22,23] A few peaks at around 20–24° were assigned as the superlattice structure of Li_2MnO_3 which has a layered structure similar to the hexagonal phase (such as $LiMO_2$) but processes a monoclinic cell belonging to the space group $C2/m$. The formation of the superlattice structure of Li_2MnO_3 was ascribed to the partial occupation of the octahedral sites in the transition metal layers by the additional Li ions.[24–26] Therefore, the lattice peaks between 20–24° were typically attributed to the alternating arrangement of Li^+ and Mn^{4+} in transition metal layers. In addition, with an increase in the molar ratios of (La, Zr) co-dopants, a peak at around 18–19° assigned to the 003 plane shifted to a lower angle, as shown in the magnified Fig. 4. This shift could be attributed to the fact that the dopants were larger (La^{3+} (1.03 Å) and Zr^{4+} (0.8 Å)) than Mn^{4+} (0.53 Å) in the Li-rich structure. Impurity peaks denoted as (*) at 32.6, 40.1 and 46.8° referred to an orthorhombic phase of $LaMnO_{3.15}$ (ICSD #89-0680) and the peaks denoted as (#) at 50.4 and 60.1° indexed with a cubic phase of $(La_{0.1}Zr_{0.9})O_{1.95}$ (ICSD #82-1011) were detected in the Li-rich structure with a high molar ratio of dopants ($x = 0.02$, pink line). A decrease in the intensity of the superlattice peak at around 21° was observed, when the molar ratio of dopants was 0.02. All of these structural changes indicated that (La, Zr) co-dopants were successfully doped into the Li-rich $Li_{1.2}Ni_{0.2}Mn_{0.6}O_2$ lattice structure and distorted the arrangement of Li^+ and Mn^{4+} ions in the transition metal layers. However, impurity phases with different lattice structures in $Li_{1.2}Ni_{0.2}Mn_{0.6-x}O_2$ with high ratio of dopants had an adverse effect on the structure stability, which coincided with the SEM observation.

3.2 Electrochemical measurement

To further evaluate the electrochemical performance of the nanorod-like $Li_{1.2}Ni_{0.2}Mn_{0.6}O_2$ electrode with or without the (La, Zr) co-dopants, CV was conducted to discuss the influence of the co-dopants on the redox reactions and phase transition processes during the first four cycles. Figure 5 shows CV plots of the $Li_{1.2}Ni_{0.2}Mn_{0.6-x}O_2$ electrodes, where the symbol x denotes the molar ratio of (La, Zr) co-dopants ($x = 0$ and 0.01). For both electrodes, three anodic peaks at around 3.90 V (A1), 4.15 V (A2), and 4.75 V (A3) and three cathodic peaks at around 4.13 V (C1), 3.65 V (C2), and 3.23 V (C3) were clearly observed. Two pairs of redox peaks at A1/C2 and A2/C1 were considered to represent the two-step reactions of Ni^{2+}/Ni^{3+} and Ni^{3+}/Ni^{4+}, indicating that the nanorod-like Li-rich $Li_{1.2}Ni_{0.2}Mn_{0.6}O_2$ electrode has electrochemical properties similar to those of the layered $LiMO_2$ (M = Ni, Co, etc.). An anodic peak at an extremely high potential of around 4.75 V (A3) was attributed to a typical sign of a phase transition of a Li_2MnO_3-like structure. This kind of phase transition was affected by the irreversible oxidation process that occurred from the charge loss of the unstable O^{2-} layer, resulting in the release of oxygen during the extraction of lithium in the transition metal layer. The phase transition only occurred in the oxidation process in the first cycle since no peaks above 4.60 V could be detected in the following cycles (Fig. S2a), which was consistent with the results reported for Li-rich materials.[27–29] In addition, the cathodic peak at a relatively low potential of around 3.23 V (C3) suggested that part of the Li_2MnO_3-like layer structure was activated during the oxidation process in the first cycle and transformed into a spinel-like phase, leading to the intercalation of lithium ions at low potential.[30] Cyclic voltammograms in the following cycles for the pristine and doped electrodes are further compared in Fig. S2. Notably, the polarization of redox pairs, representing the oxidation/reduction of Ni^{2+}/Ni^{4+}, decreased when the (La, Zr) co-dopants entered the Li-rich structure. However, there was no significant difference at a potential of 3.15 V (C3) in the following cycles. It is reasonable to consider that the (La, Zr) co-dopants in the nanorod-like Li-rich structure could effectively increase the mobility of lithium-ion and thus decrease the polarization.

To further reveal the Li^+ de-intercalation behavior in the nanorod-like $Li_{1.2}Ni_{0.2}Mn_{0.6}O_2$ electrode and electrodes doped with different ratios of (La, Zr), galvanostatic measurement was carried out under different current densities (Fig. 6). The initial charge-discharge curves within the potential range from 2.0 to 4.8 V at 0.1 C (20 mA g^{-1}) for the pristine electrode and the electrode in which the molar ratio of (La, Zr) was 0.01 are compared in Figs. 6a and 6b. The initial discharge capacity for the co-doped electrode was 210 mAh g^{-1}, which was slightly lower than that of the pristine electrode (216 mAh g^{-1}). This difference might be caused by larger heteroatoms that slightly hinder the movement of lithium ion in the initial cycle. Moreover, a plateau attributed to the phase transition of a spinel-like structure by a loss of oxygen at above 4.50 V in the initial charge plots was confirmed for both of the electrodes, which

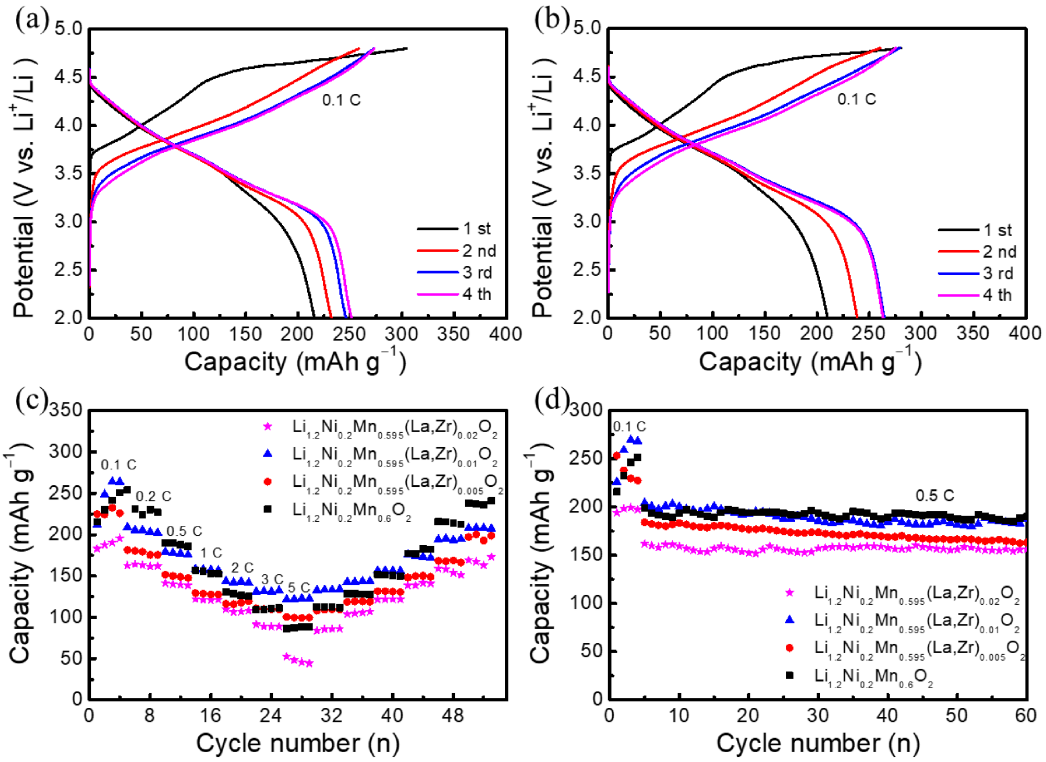

Figure 6. Galvanostatic results of nanorod-like $Li_{1.2}Ni_{0.2}Mn_{0.6-x}(La,Zr)_xO_2$. Charge-discharge curves of (a) pristine nanorod-like $Li_{1.2}Ni_{0.2}Mn_{0.6}O_2$, (b) $Li_{1.2}Ni_{0.2}Mn_{0.59}(La,Zr)_{0.01}O_2$; (c) Rate performance and (d) cycling capability at 0.5 C (100 mA g^{-1}) of the Li-rich nanorod-like electrodes with (La, Zr) co-dopants, $Li_{1.2}Ni_{0.2}Mn_{0.6-x}O_2$ ($x = 0$, 0.005, 0.01, and 0.02).

was consistent with the CV plots. However, the plateau above 4.50 V vanished for the pristine and co-doped electrodes after the first cycle and exhibited almost the same reversible capacity after sufficient activation at 0.1 C for four cycles.

Figure 6c presents the rate performance of $Li_{1.2}Ni_{0.2}Mn_{0.6-x}O_2$ with (La, Zr) co-dopants at molar ratios of $x = 0$, 0.005, 0.01, and 0.02 under different current densities from 0.1 C (20 mA g^{-1}) to 5 C (1000 mA g^{-1}). The average discharge capacities of the pristine electrode (black dots) at current densities of 0.1, 0.2, 0.5, 1, 2, 3, and 5 C were 251, 224, 189, 154, 129, 110, and 89 mAh g^{-1}, respectively. Under a current density of 1 C, the pristine nanorod-like $Li_{1.2}Ni_{0.2}Mn_{0.6}O_2$ electrode showed much higher reversible capacity than the electrode that was doped with different molar ratios of (La, Zr) co-dopants. This difference diminished with an increase in current density. However, when the current density was set at 5 C (1000 mA g^{-1}), the nanorod-like $Li_{1.2}Ni_{0.2}Mn_{0.6-x}O_2$ electrode with a molar ratio of (La, Zr) co-dopants ($x = 0.01$) achieved a stable reversible capacity of 123 mAh g^{-1}, which was much larger than that of the pristine electrode (89 mAh g^{-1}). This change suggested that an appropriate molar ratio for (La, Zr) co-dopants with a fixed molar ratio of 3 : 2 could improve the Li^+ mobility in the Li-rich structure, especially under a high current density. To confirm this assumption, cycling performance under 0.5 C (Fig. 6d) and 5 C (Fig. S3) was compared between the pristine electrode and the electrodes with different molar ratios of (La, Zr) co-dopants. Under a current density of 0.5 C for 60 cycles, the pristine electrode showed a slightly higher average reversible capacity than the (La, Zr) co-doped electrodes. However, after cycling at 5 C for 300 cycles (Fig. S3a), an obvious difference in capacity could be found between the pristine electrode and the electrode with a molar ratio of 0.01 for (La, Zr) co-dopants. In addition, compared to the capacity in the 1st cycle, the reversible discharge capacities after the 300th cycle for the pristine electrode and the electrodes with a molar ratio of 0.005 or 0.01 for (La, Zr) co-dopants were 60, 72, and 102 mAh g^{-1}, corresponding to capacity retentions of 66.7, 72.0, and 80.9 %, respectively. According to the literature, Amine and co-workers reported a $Li_{1.2}Ni_{0.2}Mn_{0.6}O_2$ materials with a self-assembled spherical hierarchical structure, showing excellent capacity retention of 67.8 % at 5 C in the 150th cycles.[31] Also, Su and co-workers reported a $Li_{1.2}Ni_{0.2}Mn_{0.6}O_2$ material fabricated by the solid-state method without structural design, showing a much lower reversible capacity of 13 mAh g^{-1} at 5 C.[32] As for this study, all of the electrodes exhibited relatively stable cycling stability and high reversible capacity, suggesting that the nanorod-like structure prepared by the MnO_2-precursor template could provide a robust three-dimensional skeleton for the reversible Li^+ de-intercalation process. A decrease in the average voltage was observed during cycling (Fig. S3b), which was attributed to the gradually formed spinel-like phase as reported in the previous literature.[33–35] Nonetheless, the nanorod-like $Li_{1.2}Ni_{0.2}Mn_{0.6-x}O_2$ with a molar ratio of 0.01 for (La, Zr) co-dopants displayed a higher average discharge potential, indicating that the (La, Zr) co-dopants could hinder the formation of the spinel-like phase from the layer structure during long-term cycling.

To further investigate the effect of the (La, Zr) co-dopants on lithium diffusion in the Li-rich structure during the charge-discharge process, the apparent lithium-ion diffusion coefficient (D_{Li^+}, $cm^2\,s^{-1}$) was used to indicate the difference in kinetics, and was calculated by the CV method. Figure 7a and S4 show the CV plots of the pristine electrode and electrodes with molar ratios of 0.005 and 0.01 for (La, Zr) co-dopants with scan rates of 0.1, 0.2, 0.3, 0.5, 0.8, and 1.0 mV s^{-1}. All of the plots at each scan rate were cycled three times and the plots obtained in the second cycle were chosen. For all of them, with an increase in the scan rate, the anodic peak shifted to a higher potential and the cathodic peak shifted to a lower potential, which increased polarization between the redox peaks. Hence, the irreversible behavior became more notable at high scan rates, which is caused by insufficient de-intercalation of Li^+ from the

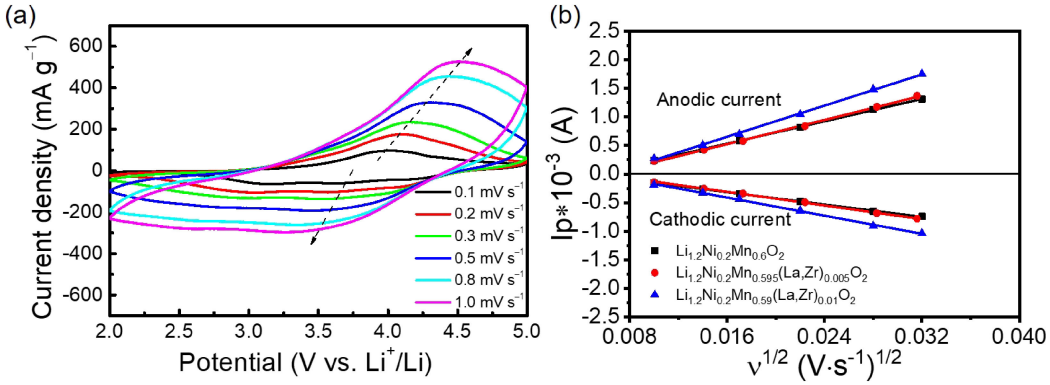

Figure 7. Kinetic analysis by CV measurement. (a) CV plots of the pristine nanorod-like $Li_{1.2}Ni_{0.2}Mn_{0.6}O_2$ electrode with different scan rate of 0.1, 0.2, 0.3, 0.5, 0.8, and 1.0 mV s^{-1}. (b) The linear fitting results of the peak current (I_p) and the square of scan rate ($\nu^{1/2}$) for $Li_{1.2}Ni_{0.2}Mn_{0.6-x}O_2$ ($x = 0$, 0.005, and 0.01), respectively.

electrode at a high rate scan. In addition, with an increase in the scan rate, the redox peaks above 4 V, which referred to the reaction of Ni^{3+}/Ni^{4+} (A2/C1), became difficult to observe and completely disappeared when the scan rate was over 0.5 mV s^{-1}. The cathodic peak (C3), representing the Li^+ insertion reaction into the gradually increased spinel-like phase, was difficult to distinguish. Besides, according to the aforementioned CV results, this peak represented the Li^+ intercalation reaction in the gradually increased spinel-like structure that did not contain the (La, Zr) co-dopants, and thus the kinetic characteristics of this phase are not discussed further. Only a pair of redox peaks, mainly representing the Ni^{2+}/Ni^{3+} reaction, denoted as A1 and C2, respectively, was used to discuss D_{Li^+} in the electrodes with different molar ratios of (La, Zr) dopants. According to Fig. 7b, a typical linear relationship between the peak current (I_p) and the square root of the scan rate ($\nu^{1/2}$) could be confirmed for all of the electrodes. This kind of relationship is typical for an intercalation reaction and can be described with the Randles-Sevick equation (Eq. 1):

$$I_p = 2.69 \times 10^5 n^{3/2} A D_{Li^+}^{1/2} C_{Li} \upsilon^{1/2} \quad (1)$$

where n is the number of electrons during the charge-transfer process, A is the contact area between the electrode and electrolyte (here, the contact area was fixed at 1.13 cm^2), and C_{Li} is the concentration of Li^+ in the electrode (4.96×10^{-2} mol cm^{-3}, calculated from the volume of the unit cell). Based on the slopes calculated from the fitting lines in Fig. 7b, the apparent lithium diffusion coefficients of the anodic peak (A1) and cathodic peak (C2) in the pristine electrode were calculated to be 1.05×10^{-11} and 3.32×10^{-12} cm^2 s^{-1}, respectively, by Eq. 1. D_{Li^+} in the nanorod-like $Li_{1.2}Ni_{0.2}Mn_{0.6-x}O_2$ electrode with molar ratios of (La, Zr) co-dopants of $x = 0.005$ and 0.01 were estimated to be 1.23×10^{-11}, 2.05×10^{-11} cm^2 s^{-1} for the anodic reaction (A1), and 3.93×10^{-12}, 6.92×10^{-12} cm^2 s^{-1} for the cathodic peak (C2), respectively. For the nanorod-like $Li_{1.2}Ni_{0.2}Mn_{0.6-x}O_2$ electrode with a molar ratio of 0.01 for (La, Zr) co-dopants, D_{Li^+} was twice that of the pristine electrode. Therefore, it could be concluded that electrodes with an appropriate molar ratio of (La, Zr) co-dopants could effectively improve the lithium-ion mobility and provide an efficient conductive route under high current density in the Li-rich layer structure.

4. Conclusion

In this work, nanorod-like Li-rich $Li_{1.2}Ni_{0.2}Mn_{0.6}O_2$ material with a three-dimensional architecture was prepared by evaporative-crystallization using nano-MnO_2 precursor as a hard template, which was pre-fabricated by a conventional hydrothermal method. In addition, heteroatoms with different molar ratios of (La, Zr) co-dopants were doped to the Li-rich structure during crystallization with a fixed ratio of 3 : 2. According to the electrochemical performance and the subsequent kinetic analysis, an appropriate molar ratio of the (La, Zr) co-dopants in the Li-rich nanorod-like $Li_{1.2}Ni_{0.2}Mn_{0.6}O_2$ electrode could reinforce the structure stability and promote Li^+ mobility with reduced polarization, which leads to an outstanding cycling performance, especially under a high current density. This study takes advantage of multiple strategies including morphology control and co-doping to provide new insight into the modification of Li-rich $Li_{1.2}Ni_{0.2}Mn_{0.6}O_2$ and other materials with relatively low ion conductivity for their application in next-generation rechargeable lithium-ion batteries.

CRediT Authorship Contribution Statement

Wencong Wang: Data curation (Lead), Validation (Lead), Writing – original draft (Lead)
Hiromasa Hanzawa: Supervision (Equal)
Ken-ichi Machida: Supervision (Equal)
Kohei Miyazaki: Supervision (Equal), Writing – review & editing (Equal)
Takeshi Abe: Supervision (Equal)

Data Availability Statement

The data that support the findings of this study are openly available under the terms of the designated Creative Commons License in J-STAGE Data listed in D1 of References.

Conflict of Interest

The authors declare no conflict of interest in the manuscript.

References

D1. W. Wang, H. Hanzawa, K. Machida, K. Miyazaki and T. Abe, *J-STAGE Data*, https://doi.org/10.50892/data.electrochemistry.17109038, (2021).
1. B. Dunn, H. Kamath, and J.-M. Tarascon, *Science*, **334**, 928 (2011).
2. S. Kim, H. Aykol, V. I. Hegde, Z. Lu, S. Kirklin, J. R. Croy, M. M. Thackeray, and C. Wolverton, *Energy Environ. Sci.*, **10**, 2201 (2017).
3. P. K. Nayak, E. M. Erickson, F. Schipper, T. R. Penki, N. Munichandraiah, P. Adelhelm, H. Sclar, F. Amalraj, B. Markovsky, and D. Aurbach, *Adv. Energy Mater.*, **8**, 1702397 (2018).
4. Z. Lu, D. D. MacNeil, and J. R. Dahn, *Electrochem. Solid-State Lett.*, **4**, A191 (2001).
5. M. Gu, A. Genc, I. Belharouak, D. Wang, K. Amine, S. Thevuthasan, D. R. Baer, J.-G. Zhang, N. D. Browning, J. Liu, and C. Wang, *Chem. Mater.*, **25**, 2319 (2013).
6. M.-H. Lin, J.-H. Cheng, H.-F. Huang, U. F. Chen, C.-M. Huang, H.-W. Hsieh, J.-M. Lee, J.-M. Chen, W.-N. Su, and B.-J. Hwang, *J. Power Sources*, **359**, 539 (2017).
7. M. M. Thackeray, C. S. Johnson, J. T. Vaughey, N. Li, and S. A. Hackney, *J. Mater. Chem.*, **15**, 2257 (2005).
8. M. H. Rossouw, D. C. Liles, and M. M. Thackeray, *J. Solid State Chem.*, **104**, 464

(1993).
9. M. H. Rossouw and M. M. Thackeray, *Mater. Res. Bull.*, **26**, 463 (1991).
10. P. Kalyani, S. Chitra, T. Mohan, and S. Gopukumar, *J. Power Sources*, **80**, 103 (1999).
11. C.-H. Shen, S.-Y. Shen, F. Fu, C.-G. Shi, H.-Y. Zhang, M. J. Pierre, H. Su, Q. Wang, B.-B. Xu, L. Huang, J.-T. Li, and S.-G. Sun, *J. Mater. Chem. A*, **3**, 12220 (2015).
12. A. Manthiram, J. C. Knight, S.-T. Myung, S.-M. Oh, and Y.-K. Sun, *Adv. Energy Mater.*, **6**, 1501010 (2016).
13. H. Yu, Y. G. So, A. Kuwabara, E. Tochigi, N. Shibata, T. Kudo, H. Zhou, and Y. Ikuhara, *Nano Lett.*, **16**, 2907 (2016).
14. R.-P. Qing, J.-L. Shi, D.-D. Xiao, X.-D. Zhang, Y.-X. Yin, Y.-B. Zhai, L. Gu, and Y.-G. Guo, *Adv. Energy Mater.*, **6**, 1501914 (2016).
15. Q. Li, G. Li, C. Fu, D. Luo, J. Fan, and L. Li, *ACS Appl. Mater. Interfaces*, **6**, 10330 (2014).
16. S. Sallard, J. Billaud, D. Sheptyakov, P. Novák, and C. Villevieille, *ACS Appl. Energy Mater.*, **3**, 8646 (2020).
17. S. Liu, Z. Liu, X. Shen, W. Li, Y. Gao, M. N. Banis, M. Li, K. Chen, L. Zhu, R. Yu, Z. Wang, X. Sun, G. Lu, Q. Kong, X. Bai, and L. Chen, *Adv. Energy Mater.*, **8**, 1802105 (2018).
18. X. Li, H. Xin, Y. Liu, D. Li, X. Yuan, and X. Qin, *RSC Adv.*, **5**, 45351 (2015).
19. J. Yang, Y. Chen, Y. Li, X. Xi, J. Zheng, Y. Zhu, Y. Xiong, and S. Liu, *ACS Appl. Mater. Interfaces*, **13**, 25981 (2021).
20. L. Li, L. Wang, X. Zhang, Q. Xue, L. Wei, F. Wu, and R. Chen, *ACS Appl. Mater. Interfaces*, **9**, 1516 (2017).
21. L. Chen, Y. Su, S. Chen, N. Li, L. Bao, W. Li, Z. Wang, M. Wang, and F. Wu, *Adv. Mater.*, **26**, 6756 (2014).
22. Y. Hinuma, Y. S. Meng, K. Kang, and G. Ceder, *Chem. Mater.*, **19**, 1790 (2007).
23. M. S. Islam, R. A. Davies, and J. D. Gale, *Chem. Mater.*, **15**, 4280 (2003).
24. A. Boulineau, L. Croguennec, C. Delmas, and F. Weill, *Chem. Mater.*, **21**, 4216 (2009).
25. D. Y. W. Yu, K. Yanagida, Y. Kato, and H. Nakamura, *J. Electrochem. Soc.*, **156**, A417 (2009).
26. Y. Koyama, I. Tanaka, M. Nagao, and R. Kanno, *J. Power Sources*, **189**, 798 (2009).
27. C. S. Johnson, N. Li, C. Lefief, J. T. Vaughey, and M. M. Thackeray, *Chem. Mater.*, **20**, 6095 (2008).
28. J.-H. Kim, M.-S. Park, J.-H. Song, D.-J. Byun, Y.-J. Kim, and J.-S. Kim, *J. Alloys Compd.*, **517**, 20 (2012).
29. Y. Chen, G. Xu, J. Li, Y. Zhang, Z. Chen, and F. Kang, *Electrochim. Acta*, **87**, 686 (2013).
30. S. F. Amalraj, B. Markovsky, D. Sharon, M. Talianker, E. Zinigrad, R. Persky, O. Haik, J. Grinblat, J. Lampert, M. Schulz-Dobrick, A. Garsuch, L. Burlaka, and D. Aurbach, *Electrochim. Acta*, **78**, 32 (2012).
31. Y. Li, Y. Bai, X. Bi, J. Qian, L. Ma, J. Tian, C. Wu, F. Wu, J. Lu, and K. Amine, *ChemSusChem*, **9**, 728 (2016).
32. Y. Liu, D. Liu, H.-H. Wu, X. Fan, A. Dou, Q. Zhang, and M. Su, *ACS Sustain. Chem. Eng.*, **6**, 13045 (2018).
33. I. Bloom, L. Trahey, A. Abouimrane, I. Belharouak, X. Zhang, Q. Wu, W. Lu, D. P. Abraham, M. Bettge, and J. W. Elam, *J. Power Sources*, **249**, 509 (2014).
34. J. R. Croy, K. G. Gallagher, M. Balasubramanian, B. R. Long, and M. M. Thackeray, *J. Electrochem. Soc.*, **161**, A318 (2014).
35. P. Oh, M. Ko, S. Myeong, Y. Kim, and J. Cho, *Adv. Energy Mater.*, **4**, 1400631 (2014).